Brazilian Journal of Physics (2025) 55:211
https://doi.org/10.1007/s13538-025-01843-5

Differentiation of Clay Content in Soil Samples Containing Clay, Silt, and Sand Using the Speckle Methodology

Sidney da Silva[1] · Gustavo Faulin[2] · Luis Zamariolli[3] · Pedro Souza[1] · Felipe Prado[4] · Niklaus Wetter[4]

Received: 9 September 2024 / Accepted: 26 June 2025 / Published online: 9 July 2025

Abstract
This study aimed to assess the textural differences in soil samples with varying percentages of clay relative to sand content. Speckle interferometry by reflection technique was used, with the aid of polarizers to increase contrast. The method was based on elements of the Time History Speckle Pattern (THSP) and Error Theory. The data consisted of videos of static and dynamic interference patterns observed on the surfaces of the soil samples. These videos were then divided into frames to create THSP files, which formed the basis for constructing the graphs that present the average relative intensities of the interference patterns over time. Quantitative results revealed that samples with higher clay content presented higher mean relative intensities compared to samples with lower clay content. The uncertainties associated with these measurements were 3.6% for the more clayey sample and 4.1% for the less clayey sample. The percentage differences between the average relative intensities were $(2.39 \pm 0.36) \times 10^{-1}$ for the highest clay percentage sample and $(3.39 \pm 0.41) \times 10^{-2}$ for the lowest clay percentage sample.

Keywords Speckle interferometry · THSP · Polarization · Soil granulometry · Error Theory elements

1 Introduction

Studying soil texture is crucial in Agricultural Engineering to discern the characteristics that impact plant growth. Among these attributes are water retention, air permeability, and displacement. A soil with a more clayey than sandy texture helps in water retention, providing greater humidity and, consequently, a more significant release of nutrients to plants, with less need for irrigation [1, 2]. Identifying soil texture is essential for defining effective management strategies and achieving optimal productivity. Exploring innovative techniques, such as Speckle analysis, holds great promise for obtaining precise quantitative results based on computational error correction from digital images.

Several published works [3–7] highlight the significant relevance of Speckle methodology in engineering and physics, particularly in the quest to comprehend contrasts and irregularities on material surfaces. In the context of soil studies for agriculture, a recent study [8] investigates the correlation between the biospeckle phenomenon [9] and varying levels of induced moisture in red-yellow argisol. The results demonstrate effective monitoring of water activity while observing different moisture levels in soil classified as red-yellow argisol.

Speckle is a subfield of optics that investigates the static or dynamic behavior of the interference phenomenon on surfaces illuminated by coherent light waves over time [10–15]. The optical technique employed for data collection is the Speckle interferometer, which can operate via reflection or refraction of light, depending on the sample type. In general, the data consist of videos that digitally record interference patterns for subsequent analysis [3, 4]. An excellent approach to comprehend the temporal evolution of the interference pattern generated by Speckle is to utilize the Time History Speckle Pattern (THSP) method. This involves segmenting a recorded video of the interference pattern into

✉ Sidney da Silva
grupoopticaaplicacoes@gmail.com

[1] Optics and Applications Group, Fatec Itaquera, São Paulo, SP 08295005, Brazil

[2] Precision Agriculture, Fatec Pompeia, Pompeia, SP 17580000, Brazil

[3] Soil and Plant Tissue Laboratory of the Nishimura Technology Foundation, Fatec Pompeia, Pompeia, SP 17580000, Brazil

[4] Energy and Nuclear Research Institute, IPEN-CNEN/SP, São Paulo 05508-000, Brazil

frames, extracting pixel lines from these frames, and organizing them to create a single image that visually represents this temporal evolution [4, 16, 17].

This work offers a quantitative alternative to improve the accuracy in the investigation of clay contents in important soil samples in agricultural production, using laser and computing as main tools and inserting a modern methodology with potential applications in agriculture. For this, we use Speckle interferometry and graphical analysis by a computational method based on the traditional methods of THSP [18, 19] and Error Theory [20, 21].

2 Theory

Figure 1 shows the photos, original (in red tones) and converted (in gray tones with intensities from 0 to 255; 8 bits), of the interference formed during the illumination of a region of a sandy soil sample using the Speckle technique by reflection using a helium–neon laser as a light source. The set of grains observed is the result of interference caused by the diffuse reflection of the laser on the surface of the material, creating a grainy effect, commonly known as Speckle.

During the process of interaction of light with the surface of the soil sample, part of the radiation will be absorbed and part emitted. The overlapping of emissions produces constructive and destructive interference, according to the interference theory of light. [10, 12–15]. Figure 2 presents a diagram of this phenomenon associated with the grains of soil constituent materials (sand, silt, and clay) important for this study.

An efficient way to understand the temporal evolution of the interference pattern produced by Speckle is to use the THSP method [4, 11, 17], which consists of recording the temporal evolution of the sample's Speckle interference patterns in a video, separating the video into frames, collecting pixel lines from each frame, and organizing them side by side, in a single image, to show the temporal evolution of this interference pattern, as shown in the diagram in Fig. 3.

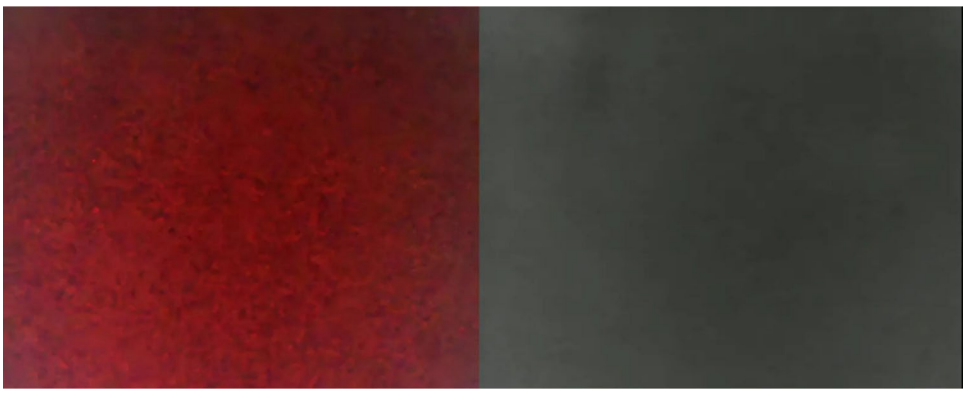

Fig. 1 Images of the static interference pattern of a soil sample using the Speckle technique by reflection with a He–Ne laser light source. Left: original image; right: image converted to grayscale

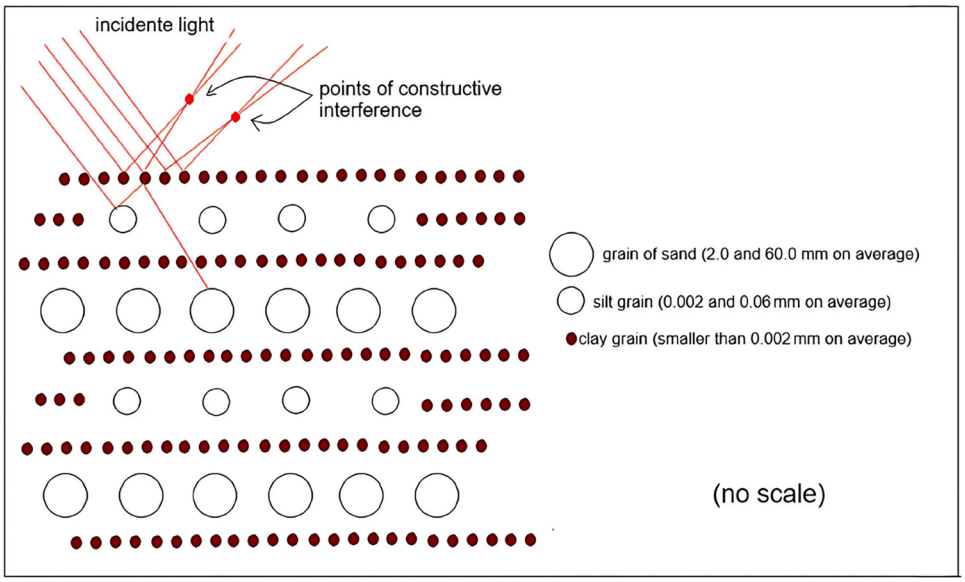

Fig. 2 Illustrative scheme of interference, by Speckle, in the constituent materials of the soil (sand, silt, and clay)

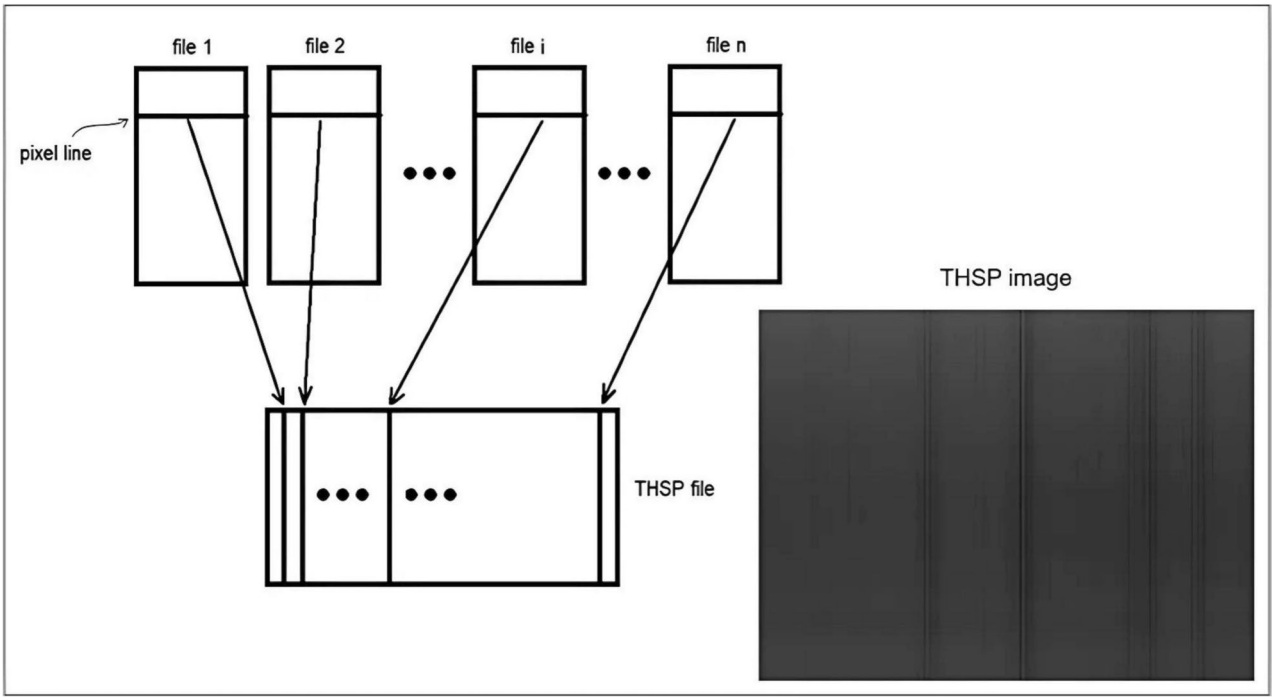

Fig. 3 Scheme of creating the THSP file and THSP image. A row of pixels from each image (frame) separated from the video is transported in order to a column in the THSP file

Each THSP file has n (lines) x m (columns) that are associated with light intensities. The relative average intensity, in each column of the THSP file, $\langle I \rangle_j$ ($j = 1, 2, \ldots, n$), is then determined by expressions (1), such that

$$\langle I \rangle_j = \frac{1}{n} \sum_{i=1}^{n} \frac{I_i}{I_{max}} \tag{1a}$$

$$\sigma_{\langle I \rangle_j} = \pm \sqrt{\frac{1}{n(n-1)} \sum_{i=1}^{n} \left(I_i - \langle I \rangle_i \right)^2} \tag{1b}$$

with $\langle I \rangle_j$ as the intensity value of each pixel, I_{max} as the maximum intensity value among the values of all pixels, for normalization purposes. $\sigma_{\langle I \rangle_j}$ is the estimated uncertainty of each $\langle I \rangle_j$, based on the Gaussian distribution theory [20, 21]. The relationship between the proportion of clay and the proportion of sand provides the relative proportionality factor, fp, of clay in relation to sand. Therefore, to calculate fp, expressions (2) are used.

$$fp = \frac{f_{clay}}{f_{sand}} \tag{2a}$$

$$\sigma_{fp} = \pm fp \sqrt{\left(\frac{\sigma_{f_{clay}}}{f_{sand}} \right)^2 + \left(\frac{\sigma_{f_{sand}}}{f_{sand}} \right)^2} \tag{2b}$$

with f_{clay} and f_{sand} as the respective proportion values of clay and sand. $\sigma_{f_{clay}}$ and $\sigma_{f_{sand}}$ are the respective uncertainties of f_{clay} and f_{sand}.σ_{fp} is the estimated uncertainty of fp, from Gaussian distribution theory [20, 21]. To contrast the distributions of relative intensities of samples with higher clay content in relation to samples with lower clay content, it is necessary to normalize the $\langle I \rangle_j$ values since the proportions (p_{clay} or p_{sand}) of these materials in the available samples were not the same. Thus, when comparing two samples, the following average adjustment factors were proposed:

$$\langle f \rangle_{\text{more (or less) clay}} = \frac{p_{more}}{p_{sand}} \tag{3a}$$

$$\sigma_{\langle f \rangle_{\text{more (or less) clay}}} = \pm \langle f \rangle_{\text{more (or less) clay}} \sqrt{\left(\frac{\sigma_{p_{clay}}}{p_{clay}} \right)^2 + \left(\frac{\sigma_{p_{sand}}}{p_{sand}} \right)^2} \tag{3b}$$

with $\sigma_{\langle f \rangle_{\text{more (or less) clay}}}$ as the estimated uncertainty of the average value $\langle \langle f \rangle_{\text{more (or less) clay}}$ from the uncertainty propagation theory [20, 21].

Another normalization factor, important for contrasting the distributions of the relative average intensities of the samples, considered environmental conditions, such as temperature (T), pressure (P), and humidity (H). Thus, using the weighted average.

$$f_{\text{environmental factor}} = f_{\text{T}} + f_{\text{P}} + f_{\text{H}} \tag{4a}$$

$$\sigma_{f_{\text{environmental factor}}} = \pm\sqrt{{\sigma_{f_{\text{T}}}}^2 + {\sigma_{f_{\text{P}}}}^2 + {\sigma_{f_{\text{H}}}}^2} \tag{4b}$$

$$f_{\text{condition}} = \alpha_{\text{condition}} \frac{\langle \text{condition} \rangle_{\text{i}}}{\langle \text{condidion} \rangle} \tag{4c}$$

$$\sigma_{f_{\text{condition}}} = \pm f_{\text{condition}} \sqrt{\left(\frac{\sigma_{\alpha_{\text{condition}}}}{\alpha_{\text{condition}}}\right)^2 + \left(\frac{\sigma_{\langle \text{condition} \rangle_{\text{i}}}}{\langle \text{condition} \rangle_{\text{i}}}\right)^2 + \left(\frac{\sigma_{\langle \text{condition} \rangle}}{\langle \text{condition} \rangle}\right)^2} \tag{4d}$$

With f_{T}, f_{P}, and f_{H} as the weighted factors T, P and H, respectively, and T, P, or H as the condition. $\langle T \rangle_{\text{i}}$, $\langle P \rangle_{\text{i}}$, and $\langle U \rangle_{\text{i}}$ are the average values of all collections, and $\langle T \rangle$, $\langle P \rangle$, and $\langle H \rangle$ are the average values of all collections of the aforementioned quantities. The coefficients α_{T}, α_{P}, and α_{H} represent partial normalizations for each quantity, such that

$$\alpha_{\text{condition}} = \frac{(\text{condition})_{\text{max}} - (\text{condition})_{\text{min}}}{(\text{condition})_{\text{max}}} \tag{5a}$$

$$\sigma_{\alpha_{\text{condition}}} = \pm \alpha_{\text{condition}} \sqrt{\frac{{\sigma_{(\text{condition})_{\text{max}}}}^2 + {\sigma_{(\text{condition})_{\text{min}}}}^2}{\left(T_{(\text{condition})_{\text{max}}} - T_{(\text{condition})_{\text{min}}}\right)^2} + \left(\frac{\sigma_{(\text{condition})_{\text{max}}}}{T_{(\text{condition})_{\text{max}}}}\right)^2} \tag{5b}$$

$(\text{condition})_{\text{max}}$ and $(\text{condition})_{\text{min}}$ are the maximum and minimum conditions (T, P, or H) among all measurements.

To normalize the relative average intensities, the factors are used as follows:

The uncertainties of expressions (4) and (5) were estimated based on the uncertainty propagation theory [20, 21].

$$\langle I \rangle_{\text{j-normal}} = \langle I \rangle_{\text{j}} \langle f \rangle_{\text{more (or less clay)}} f_{\text{environmental factor}} \tag{6a}$$

$$\sigma_{\langle I \rangle_{\text{j-normal}}} = \pm \langle I \rangle_{\text{j-normal}} \sqrt{\left(\frac{\sigma_{\langle I \rangle_{\text{j}}}}{\langle I \rangle_{\text{1}}}\right)^2 + \left(\frac{\sigma_{\langle f \rangle_{\text{more (or less clay)}}}}{\langle f \rangle_{\text{more (or less clay)}}}\right)^2 + \left(\frac{\sigma_{f_{\text{environmental factor}}}}{f_{\text{environmental factor}}}\right)^2} \tag{6b}$$

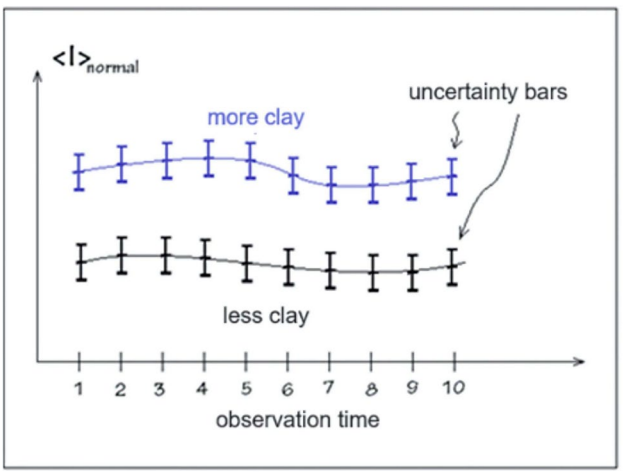

Fig. 4 Contrast curves between distributions of normalized mean relative intensities between samples with higher (blue distribution) and lower (black distribution) clay concentrations. Solid lines are guides and do not represent the true function of the distribution

Figure 4 presents an illustrative diagram of the graph that will represent the distributions of normalized relative intensities, $\langle I \rangle_{\text{j-normal}}$, of the contrasted samples.

3 Methodology

3.1 Soil Samples

The work carried out used soil samples with higher and lower percentages of clay, identified by codes 111214/9 and 106489/4, respectively, as shown in the photos in Fig. 5.

Soil particles exhibit varying proportions of sand, silt, and clay, with the soil texture being determined by the relative proportion of these components. These components are classified based on particle size, with sand particles. The samples with the highest clay content were labeled with code 111214/9, while those with the lowest clay percentage were designated as code 106489/4, having diameters ranging from 0.05 to 2 mm, silt particles having diameters ranging

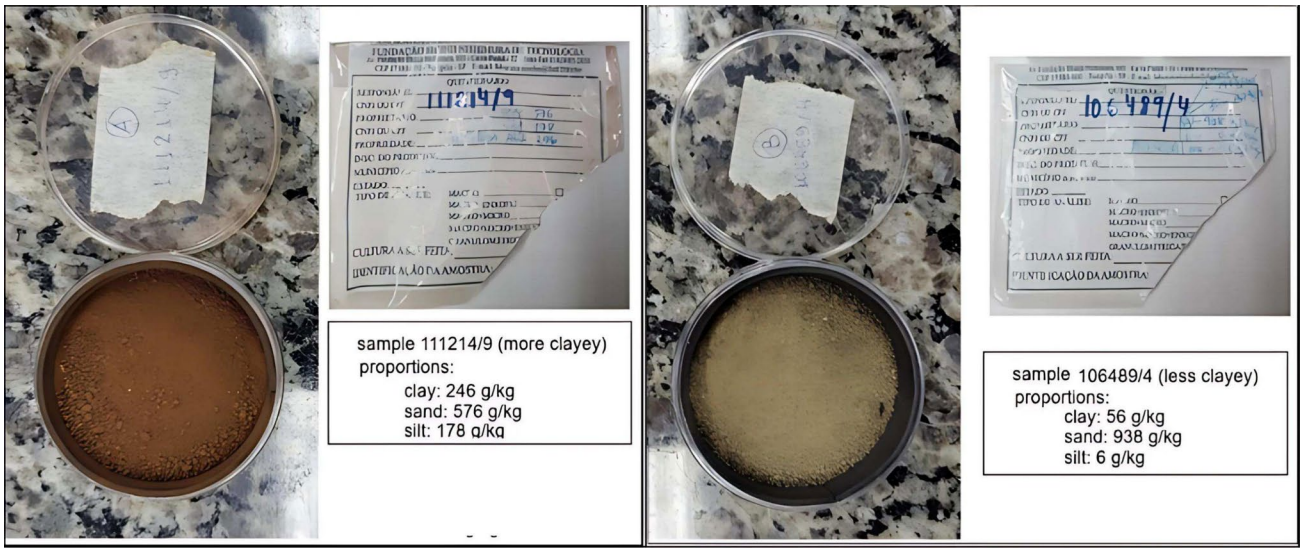

Fig. 5 Soil samples: more clayey (111214/9); less clayey (106489/4)

from 0.002 to 0.05 mm, and clay particles having diameters smaller than 0.002 mm [22].

The samples were initially prepared according to standard recommendations in the area of agronomy, [23, 24] by researchers Prof. Dr. Gustavo Di Chiacchio Faulin and Prof. Me. Luis Eduardo Rissato Zamariolli from the Soil and Plant Tissue Laboratory of the Nishimura Technology Foundation of Fatec Pompéia, the result of a partnership between the Optics and Applications Laboratory of Fatec Itaquera and the Soil Laboratory of Fatec Pompeia. The pipette technique [22–24] was used, essential for determining the soil particle size, which determined the distribution of particles with a diameter of less than 2.0 mm. Initially, a soil sample is dispersed in a NaOH solution and shaken vigorously to promote particle dispersion. Then, the NaOH solution is transferred to an Erlenmeyer flask, which is shaken for 16 h. The sand fraction is separated by sieving and washed with distilled water to retain the sand and deposit the clay and silt in a beaker. The sand goes through an oven drying process, and its mass is then measured. The beaker is filled with distilled water, and the solution settles. After sedimentation, the solution is removed with a pipette and transferred to a crucible, which is taken to the oven for drying, separating the clay fraction. The silt fraction is calculated as the difference between the sand fraction and the clay fraction. The samples were adapted and positioned in acrylic boxes with black EVA (ethylene vinyl acetate) coating to reduce light dispersion by researchers from the Optics and Applications Laboratory of Fatec Itaquera.

3.2 Technique

The optical technique employed was an experimental configuration of the Speckle interferometer by reflection, which incorporated two linear polarizers. This setup is depicted in the photograph in Fig. 6.

This technique involves observing samples and producing images with interference patterns. From the point of view of wave optics, the laser light (1) emitted by a helium–neon (He–Ne) source passes through a spatial filter (2). This filter consists of an objective lens (2.1) and a pinhole (2.2), which

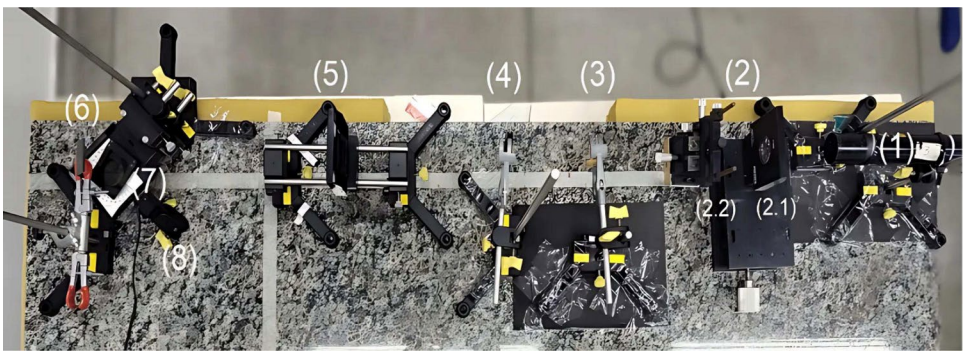

Fig. 6 Photo of the experimental setup: Speckle reflection interferometer with linear polarizers

Table 1 Proportions of clay, sand, and silt in soil samples used in data collection

Samples	Sand (g kg^{-1})	Silt (g kg^{-1})	Clay (g kg^{-1})	USDA(*) soil texture classification [22]
106489/4	938.0 ± 0.5	6.0 ± 0.5	56.0 ± 0.5	Sand
111214/9	576.0 ± 0.5	178.0 ± 0.5	246.0 ± 0.5	Sand loam

(*) United States Department of Agriculture

together transform the Gaussian spatial wave into a spherical one. Subsequently, the light passes through a plano-convex lens (3), converting it into a plane wave. This transformation aligns the light rays in parallel, allowing better control over the light used in the experiment. Additionally, it simplifies the mathematical analysis by enabling interpretation within an inertial system of Cartesian coordinates. Continuing the process, the resulting light then passes through an iris (4), which selects the appropriate diameter for observation. Then, the first linear polarizer (5) determines a specific direction for the light, which goes to a flat mirror (6). The mirror directs the light to the sample, allowing the interference pattern to be obtained. Subsequently, a digital camera (8) captures this pattern after passing through the second polarizer (7), known as an analyzer, which modifies the polarization state of the light to increase contrast and intensity. Finally, videos are stored as digital files on a computer.

The data capture process was organized as follows:

(i) Three data collections were conducted, labeled as Collection A (involving static samples), Collection B (involving samples in uniform circular motion at an approximate frequency of 0.2 cycles per second), and Collection C (involving samples in uniform circular motion at an approximate frequency of 0.5 cycles per second).
(ii) For each data collection (A, B, or C), x videos were recorded for each sample, with a time interval Δt representing the exposure of the resulting light in each video. Additionally, during each data collection, the essential environmental parameters, including temperature, pressure, and humidity, were measured n;
(iii) The videos and the values of environmental conditions were stored in files.

Table 2 Relative factors of proportionality of the amount of clay in relation to the sand

Sample	Proportionality factors (fp)
106489/4 (less clayey)	0.0597 ± 0.0005
111214/9 (more clayey)	0.4270 ± 0.0009

3.3 Method

The main objective of the developed method was to present quantitative graphical results from the computational calculation of relative average intensities as a function of sample exposure time. The theories that supported the computational method were associated with the traditional THSP and Error Theory methods, according to what was presented in Sect. 2.

The procedures for the analysis were as follows:

(i) From the concentration data provided by the researchers who prepared the samples, the clay proportionality factors were determined in relation to the sand for each sample, together with their corresponding uncertainties, according to expressions (2) and (3), presented in Sect. 2.
(ii) Environmental values were measured during data collection. Each magnitude was measured 10 times, and uncertainties were determined by combining the statistical uncertainty with the uncertainties associated with the measuring instruments, following the principles of Error Theory [20, 21], according to expressions (4) and (5), presented in Sect. 2.
(iii) With this, the average environmental factors were determined for each sample collection;
(iv) Each video was cut into the 30-s mark, disregarding the beginning and end of the collection, to eliminate most of the instabilities;
(v) Each cropped video was separated (24 fps) into image frames that were used in determining the THSP file;
(vi) Each frame was converted to gray scale with intensities from 0 to 255, in 8 bits, to obtain a unique matrix of intensities without loss of generality and information for this work;
(vii) In each frame,
  (a) one horizontal line of pixels was removed from the same position;
  (b) As explained in the theory part (Sect. 2), each line was arranged vertically, in sequence, to produce the THSP files.
(viii) In each THSP file,
  (a) the relative average intensities were calculated from the algorithms of expressions (1) and (2), presented in Sect. 2.
  (b) the normalizations of proportions of relative average intensities were calculated, according to expression (6), presented in Sect. 2.
  (c) final adjustments of relative mean intensities were performed.

Table 3 Proportionalities for the environmental conditions of the three data collections

Greatness for environmental factors	Collection A (static)	Collection A (slow dynamics)	Collection A (fast dynamics)
Average temperature ($<T>$) (°C)	14.7 ± 0.3	19.0 ± 0.3	21.2 ± 0.3
Average pressure ($<P>$) (hPa)	983 ± 10	1027 ± 11	1008 ± 12
Average relative humidity ($<U>$) (%)	63 ± 6	73 ± 6	54 ± 6

(ix) Construction of graphics, like the model in Fig. 4:

(a) The final relative average intensities were graphically organized in function to the observation times;
(b) In the same graph, the distributions of a sample with more and less clay content were contrasted.

4 Results

The proportions of clay, sand, and silt for these samples are shown in Table 1.

In the technique in Fig. 1, the laser employed had a wavelength of 632.8 nm and a power of 21 mW. The spatial filter assembly consisted of a $\times 10$ magnification microscope objective and a pinhole aperture with a diameter of 25 µm. The diameter of the light beam, determined by the iris, was $(2.0 \pm 0.2) \times 10$ m. For each data collection (A, B, or C) conducted on different days, three videos were recorded for each sample, with approximately 40 s of exposure to the resulting light per video. A time interval of 30 s was selected for all videos. The cuts were made between the time points 5 and 35 s.

The proportionality factors for clay in relation to sand were calculated based on data from samples 106489/4 (with lower

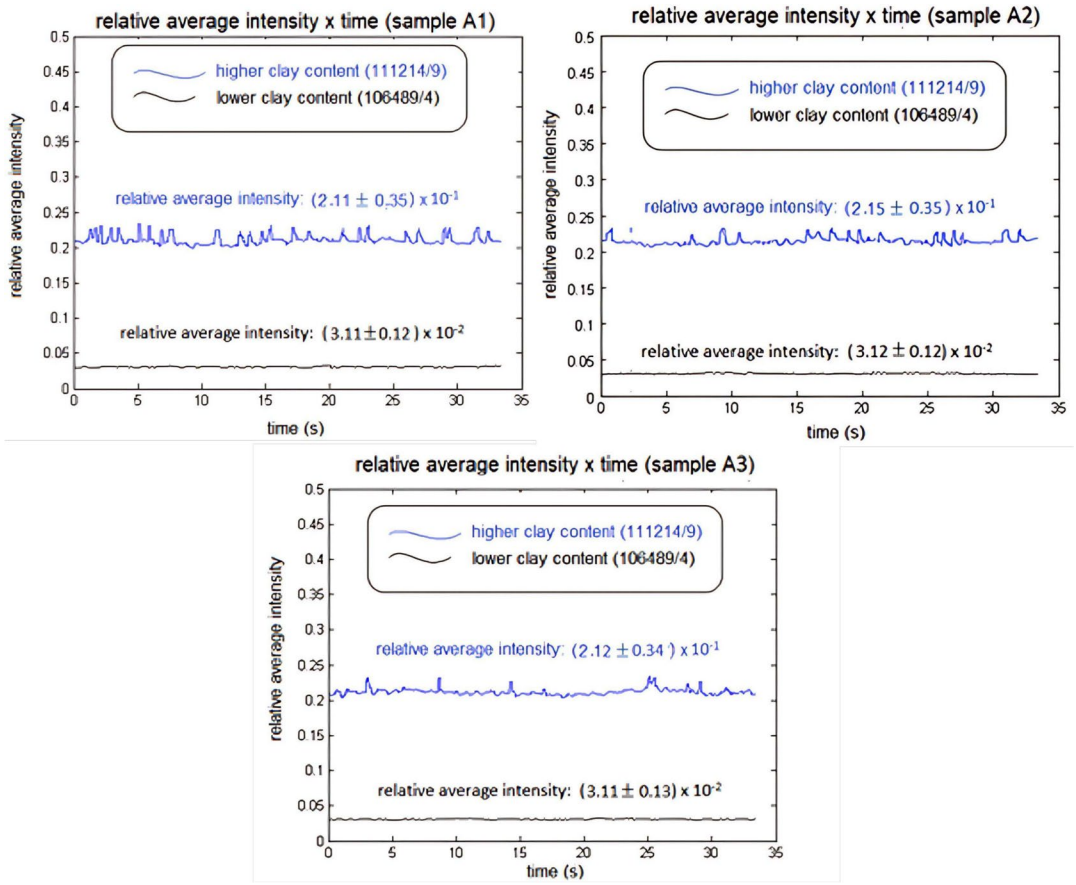

Fig. 7 Distributions of normalized mean relative intensities versus observation times of Speckle interferences from the A1, A2, and A3 videos of collection (static) for samples with more (in blue) and less (in black) proportion of clay. The blue and black lines are guides to indicate distribution swings visually

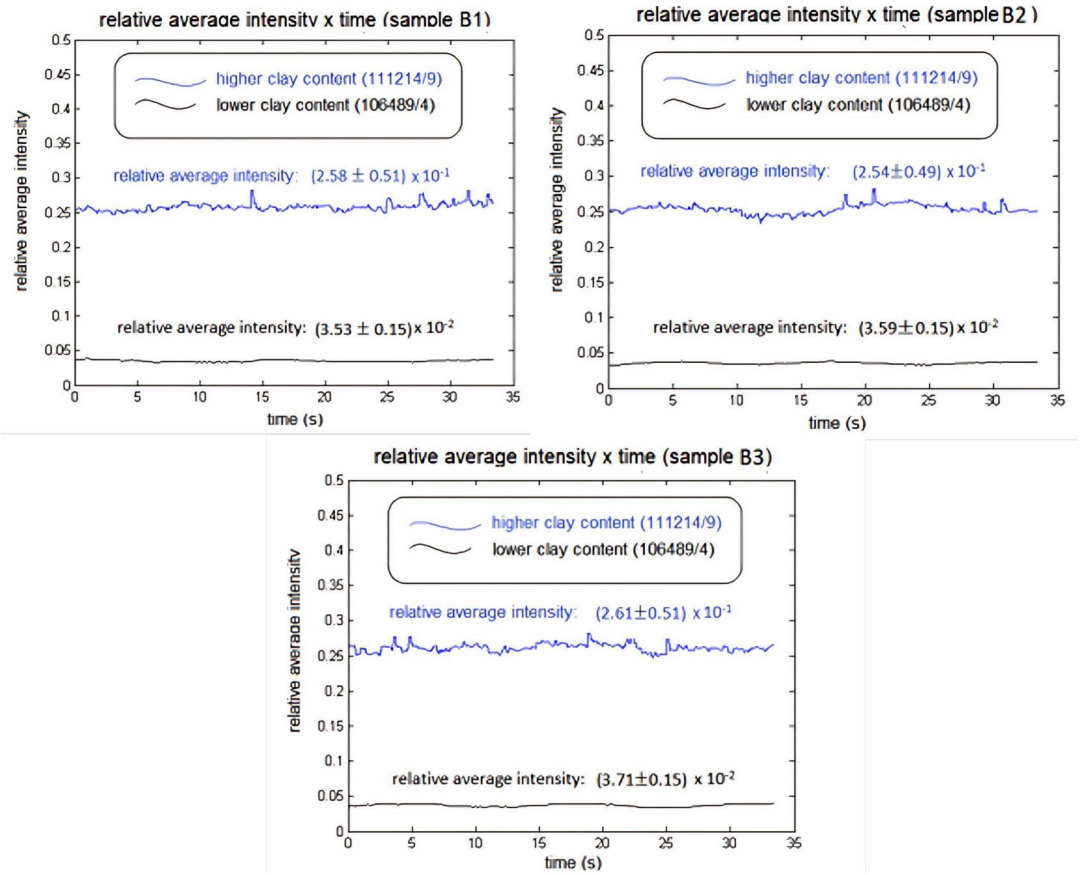

Fig. 8 Distributions of normalized mean relative intensities versus observation times of Speckle interferences from the B1, B2, and B3 videos of collection (lower dynamics) for samples with more (in blue) and less (in black) proportion of clay. The blue and black lines are guides to indicate distribution swings visually

clay content) and 111214/9 (with higher clay content). Table 2 presents these values, along with their respective uncertainties.

The average values and uncertainties of the environmental conditions, temperature, pressure, and humidity are shown in Table 3.

The graphs, which display the distributions of average relative intensities normalized as a function of observation times, reveal the results of Speckle interference contrasts between samples with varying proportions of clay.

These graphs were generated from data from three different collections: A (static) (Fig. 7), B (slow dynamics) (Fig. 8), and C (fast dynamics) (Fig. 9). The graphs were created using computer programs developed in the Optics and Applications laboratory, employing algorithms based on Error Theory and THSP Theory [20, 21].

5 Discussion

In all distributions, it is evident that the normalized relative average intensities are consistently higher for samples with greater clay content (indicated by the blue distributions). This phenomenon highlights a more pronounced Speckle interference activity in these samples. Although the mean values of the distributions for each set (A, B, and C) do not precisely match up to the second decimal place, the associated uncertainties maintain them statistically equivalent within an acceptable tolerance for each result.

The distributions for samples of type C (fast dynamics) exhibit greater variation compared to those for samples of type B (slow dynamics) and, subsequently, to those of type A (static). This occurs because the movement produces an increase in Speckle interference. However, the movement with controlled average speed remained the same as the verification of contrast between the samples, with more and less clay content.

From the point of view of interferometry, it is possible to observe greater production of constructive interference in samples containing a higher clay content, compared to samples containing a lower clay content. This is possible due to the differences between the grain sizes of clay, silt, and sand. Although the granulometric analysis associated with Speckle interference was not conducted in this study, its inclusion in future work could serve to reinforce and validate the results presented here.

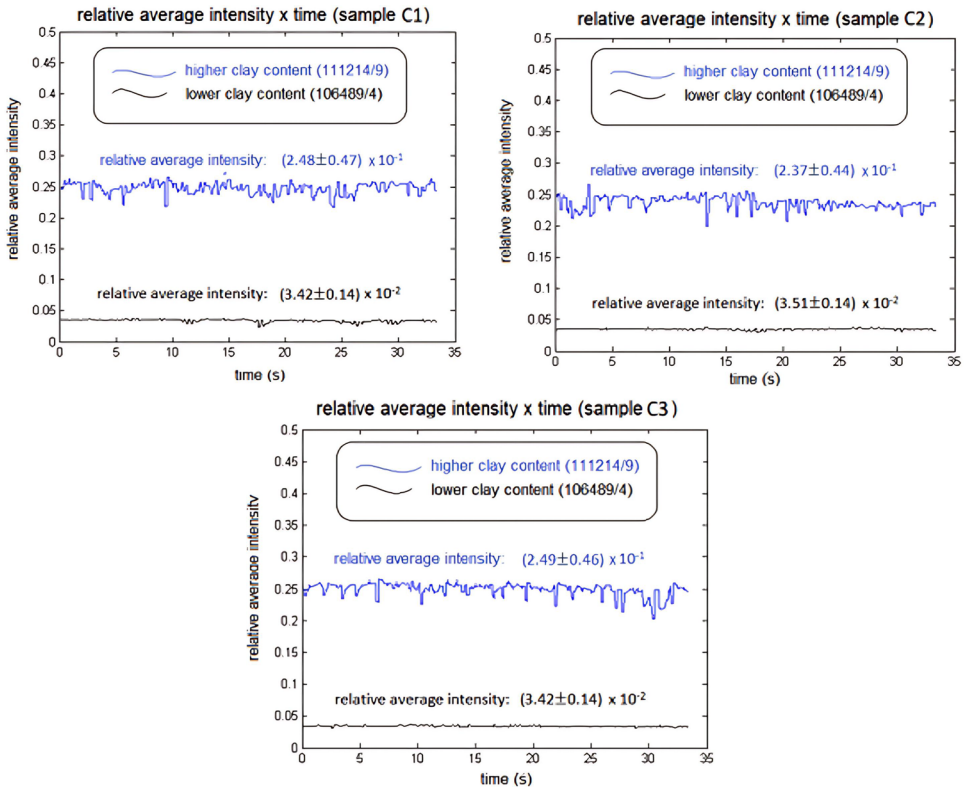

Fig. 9 Distributions of normalized average relative intensities versus observation times of Speckle interferences from the C1, C2, and C3 collection videos (fast dynamics) for samples with more (in blue) and less (in black) proportion of clay. The blue and black lines are guides to indicate distribution swings visually

Compared to the traditional methodology [1], the data collection and analysis process are more efficient and faster with the Speckle methodology, providing the possibility of using a greater number of samples and, therefore, producing greater accuracy. However, it will be necessary to carry out additional measurements and analyses using a larger set of samples to enable a more robust comparison between the methodology proposed here and the traditional approaches currently used by farmers.

6 Conclusions

All graphs showed higher average relative intensity for higher clay content (samples 111214/9) in relation to lower clay content (samples 106489/4). Therefore, there are differences between the greater or lesser amount of clay in the samples, identified by the Speckle pattern. The methodology was efficient and presented a possible alternative to the soil contrast study. Future work could classify the average percentage amounts of clay, silt, and sand in different samples to build a soil contrast map. Over time, feed a database with values of relative intensities and build an artificial intelligence program to identify the percentages of these mineral materials in uncatalogued soils.

Acknowledgements Grateful for the financial support from the São Paulo Research Foundation (2012/18162-4, 2019/23700-4, 2022/15276-0); Physical support from the Faculty of Technology of Pompeia (Fatec Pompeia), Faculty of Technology of Itaquera (Fatec Itaquera), Faculty of Technology of São Paulo and Institute of Energy and Nuclear Research of São Paulo (IPEN-SP).

Author Contribution The authors are grateful for the financial support from Fundação de Amparo à Pesquisa do Estado de São Paulo (2012/18162–4, 2019/23700–4, 2022/15276–0); The physical support from Faculdade de Tecnologia de Pompeia (Fatec Pompeia), Faculdade de Tecnologia de Itaquera (Fatec Itaquera) and Instituto de Pesquisas Energéticas e Nucleares de São Paulo (IPEN-SP). Co-authors Gustavo Di Chiacchio Faulin and Luís Eduardo Zamariolli contributed to the preparation of soil samples. The lead author (Sidney Leal da Silva) contributed theory, data, and analysis. The other co-authors helped with the preparation and first revisions of the article.

Funding Grateful for the financial support from the São Paulo Research Foundation (2012/18162–4, 2019/23700–4, 2022/15276–0); Physical support from the Faculty of Technology of Pompeia (Fatec Pompeia), Faculty of Technology of Itaquera (Fatec Itaquera), Faculty of Technology of São Paulo, and Institute of Energy and Nuclear Research of São Paulo (IPEN-SP).

Data Availability https://drive.google.com/drive/folders/1inQIGernWqO6AzfZ4ilF883eEE1Q7FWQ?usp=drive_link.

Declarations

Conflict of Interest The authors declare no competing interests.

Use of AI Tools Declaration The authors declare they have not used Artificial Intelligence (AI) tools in the creation of this article.

References

1. L.N. Centeno, M.D.F. Guevara, S.T. Cecconello, R.O.D. Souza, L.C. Timm, Textura do solo: conceitos e aplicações em solos arenosos. Revista Brasileira de Engenharia e Sustentabilidade (Pelotas - RS) **4**(1), 31–37 (2017)
2. V.A. Klein, M. Baseggio, T. Madalosso, C.D. Marcolin, Textura do solo e a estimativa do teor de água no ponto de murcha permanente com psicrômetro. Cienc. Rural. **40**(7), 1550–1556 (2010)
3. G.D.C. Faulin, R.A. Da Silva, G.A.L. Junior, R.C.M.S. Contini, S.L. Da Silva, Aplicação da Metodologia Speckle na investigação da classe textural do solo. Congresso Brasileiro de Agricultura de Precisão, ConBAP. Campinas, (2022)
4. S.L. Da Silva et al., Determinação de propriedades mecânicas do aço 1010 sob tensão no regime elástico por meio de *Speckle* dinâmico. Revista Brasileira de Física Tecnológica Aplicada **4**(1), 1–15 (2017). https://doi.org/10.3895/rbfta.v4n1.5406
5. M.M. Marchiori, A.J. De Souza, Estudo para a proposição de um novo método de medição de rugosidade baseado em reflexão difusa de LASER. In: 7º Congresso Brasileiro de Engenharia de Fabricação. Associação Brasileira de Engenharia e Ciências Mecânicas (2013)
6. R.D.P. Junior, M. Muramatsu, Desenvolvimento de um rugosímetro a LASER. Revista de Física Aplicada e Instrumentação. **17**(2), (2004). ISSN: 0102–6895
7. D. Prazak, M. Ohlidal, Laser Speckle spectral correlation and surface roughness. In: 12th Czech-Slovak Polish Optical Conference on Wave and Quantum Aspects of Contemporary Optics. International Society for Optics and Photonics, p. 339–347, (2001)
8. L.D.V. Santos, A.M. Enes, F.S.R. Holanda, C.V.S. Oliveira, A. Pedroti, Avaliação do comportamento do biospeckle em diferentes níveis de umidade do solo. Brasilian J. Develop. **6**(7), 52891–52908 (2020). https://doi.org/10.34117/bjdv6n7-892
9. J.A. Alves, Aplicação da técnica de biospeckle laser com abordagem espectral em cenoura minimamente processada. 74 f. Tese (Doutorado em Ciência dos Alimentos) – Universidade Federal de Lavras, 2012. Repositório: https://docplayer.com.br/124604768-Juliana-alvarenga-alves-aplicacao-da-tecnica-do-biospeckle-laser-com-abordagem-espectral-em-cenoura-minimamente-processada.html
10. B.E.A. Saleh, M.C. Teich, Fundamentals of photonics. Second edition. Canada: John Wiley & Sons, Inc., 1177 p., 2007
11. E.R. Da Silva, M. Muramatsu, O fenômeno do *Speckle* como introdução à metrologia óptica no laboratório didático. Rev. Bras. Ensino Fis. **29**(2), 283–286 (2007)
12. M. Ferreira, Óptica e Fotónica. Primeira Edição. Lisboa: Lidel-Edições Técnicas, 438 p., 2003. ISBN: 972757288X
13. E. Hecht, Óptica. Segunda Edição, Lisboa, Portugal. Fundação Calouste Gulbenkian, 2002. ISBN: 9723109670
14. R.D. Guenther, Modern optics. United States of America. John Wiley & Sons, 1990. ISBN: 0471605387
15. K.J. Gasvik, Optical metrology. Third Edition. England: John Wiley & Sons Ltd., 360 p., 2002. ISBN: 9780470843000
16. S.L. Da Silva, Estudo das tensões em amostras fotoelásticas com Holografia Digital – Análise quantitativa. Primeira Edição. São Paulo: Novas Edições Acadêmicas, 142 p., 2017. ISBN: 978–3–330–75868–1
17. D.J.F. Lucena, M.C. Oliveira, J. Ferreira, E. Lima, Caracterização de atividade biológica usando análise de texturas em Speckle. SIBGRAPI. https://researchgate.net/publication/263336725
18. R. Arizaga, M. Trivi, H. Rabal, Speckle time evolution characterization by the co-occurrence matrix analysis. Opt. Laser Technol. **31**(2), 163–169 (1999). https://doi.org/10.1016/S0030-3992(99)00033-X
19. V.R. Vanin, P. Gouffon, O.A.M. Helene, Tratamento Estatístico de Dados em Física Experimental. 2ª Edição. São Paulo: Editora Edgard Blucher Ltda, 116 p., 1991. ISBN: 9788521200062
20. J.H. Vuolo, Fundamentos da Teoria de Erros. 2º edição. São Paulo: Editora Edgard Blucher Ltda, 264 p., 1996. ISBN: 9788521200567
21. D.F. Brisola, T.L.A.P. Fernandes, Otimização no preparo de amostras para a análise em espectrofotômetro de fluorescência de raios X, XVI Jornada de Iniciação Científica - CETEM, (2008)
22. M.E.C.C. Paula, M.N. Duarte, M.E.C. Claessen, W.O. Barreto, Manual de métodos de análise de solo. Segunda edição. Rio de Janeiro, Centro Nacional de Pesquisas do Solo da Embrapa, 212 p., 1997. ISBN: 85–85864–03–6
23. A.R. Nogueira, de A. Preparo de amostras, VIII Encontro Nacional sobre Métodos dos Laboratórios da Embrapa, (2003)
24. USDA Soil Survey Manual. Soil survey staff, soil conservation service. U.S. Department of Agriculture handbook 18, U.S. Department of Agriculture, Washington, DC, 437 p., 1993
25. R. Nassif, C.A. Nader, F. Pellen, G.L. Brun, M. Abboud, B.L. Jeune, Retrieving controlled motion parameters using two speckle pattern analysis techniques: spatiotemporal correlation and the temporal history speckle pattern. Appl. Opt. **52**(31), 7564–7569 (2013). https://doi.org/10.1364/AO.52.007564